electronics

MDPI

Article

Hybrid Precoding Algorithm for Millimeter-Wave Massive MIMO-NOMA Systems

Samarendra Nath Sur [1], Debdatta Kandar [2], Adão Silva [3], Nhan Duc Nguyen [4,*], Sukumar Nandi [5] and Dinh-Thuan Do [6]

[1] Department of Electronics and Communication Engineering, Sikkim Manipal Institute of Technology, Sikkim Manipal University, Gangtok 737136, Sikkim, India; samar.sur@ieee.org
[2] Department of Information Technology, North Eastern Hill University, Shillong 793022, Meghalaya, India; kdebdatta@gmail.com
[3] Instituto de Telecomunicações (IT), Departamento de Eletrónica, Telecomunicações e Informática (DETI), University of Aveiro, 3810-193 Aveiro, Portugal; asilva@av.it.pt
[4] Faculty of Mechanical-Electrical and Computer Engineering, School of Engineering and Technology, Van Lang University, 69/68 Dang Thuy Tram Street, Ward 13, Binh Thanh District, Ho Chi Minh City 70000, Vietnam
[5] Department of Computer Science, Indian Institute of Technology Guwahati, Guwahati 781039, Assam, India; sukumar@iitg.ernet.in
[6] Department of Computer Science and Information Engineering, College of Information and Electrical Engineering, Asia University, Taichung City 41354, Taiwan; dodinhthuan@asia.edu.tw
* Correspondence: nhan.nd@vlu.edu.vn

Abstract: In this paper, the performance of the millimeter-wave (mmWave) massive multiple-input multiple-output (mMIMO) non-orthogonal multiple access (NOMA) systems is investigated under multiple user scenarios. The performance of the system has been analyzed in terms of spectral efficiency (SE), energy efficiency (EE), and computational complexity. In the case of the mMIMO system, the linear precoder with matrix inversion becomes less efficient due to its high computational complexity. Therefore, the design of a low-complex hybrid precoder (HP) is the main aim of this paper. Here, the authors have proposed a symmetric successive over-relaxation (SSOR) complex regularized zero-forcing (CRZF) linear precoder. Through simulation, this paper demonstrates that the proposed SSOR-CRZF-HP performs better than the conventional linear precoder with reduced complexity.

Keywords: hybrid precoder (HP); non-orthogonal multiple access (NOMA); massive MIMO (mMIMO); channel capacity; energy efficiency; computational complexity

check for updates

Citation: Sur, S.N.; Kandar, D.; Silva, A.; Nguyen, N.D.; Nandi, S.; Do, D.-T. Hybrid Precoding Algorithm for Millimeter-Wave Massive MIMO-NOMA Systems. *Electronics* **2022**, *11*, 2198. https://doi.org/10.3390/electronics11142198

Academic Editor: Athanasios Kanatas

Received: 1 June 2022
Accepted: 11 July 2022
Published: 13 July 2022

Publisher's Note: MDPI stays neutral with regard to jurisdictional claims in published maps and institutional affiliations.

Copyright: © 2022 by the authors. Licensee MDPI, Basel, Switzerland. This article is an open access article distributed under the terms and conditions of the Creative Commons Attribution (CC BY) license (https://creativecommons.org/licenses/by/4.0/).

1. Introduction

Future generation communication systems are looking for high-speed and low-latency characteristics in the system. To fulfill this goal, millimeter-wave (mmWave) communication combined with massive multiple-input multiple-output (mMIMO) plays a significant role [1]. The mmWave-mMIMO system enhanced the spectral efficiency (SE) and energy efficiency (EE) of the system tremendously by exploiting huge available bandwidth in the mmWave frequency bands and high multiplexing gains. Because of the potential of the mmWave-mMIMO system, it is considered to be a promising solution for the future generation of wireless communication systems [2]. Generally, three architectures of mmWave mMIMO systems are thoroughly investigated. These are commonly known as, fully digital (FD) architecture, fully connected (FC) architecture, and sub-connected (SC) architecture. For FD architecture, each antenna is associated with a dedicated RF chain. For such a large antenna system, a conventional MIMO system with fully digital signal processing makes the system unrealizable as the cost, energy consumption and complexity of the system become unaffordable [3–5]. To deal with this issue, hybrid precoding (HP) has

been proposed [6–8] and its performance has been evaluated over the years. As in [9], the authors have demonstrated that by utilizing HP one can achieve the same performance by significantly reducing the number of required RF chains in mmWave mMIMO systems. FC and SC architectures are generally considered part of HP design. In the case of FC architecture, fewer RF chains are used and each RF chain is connected to all the antennas. However, in the case of an SC architecture, each of the RF chains is associated with a subset of the total number of antennas.

The performance of the mmWave-mMIMO system is generally evaluated in terms of SE, EE, computational complexity, etc. The analysis of EE becomes particularly important in the case of the massive antenna system. The zero-forcing (ZF) and minimum mean squared error (MMSE) are two very commonly used linear precoder schemes for the mMIMO system. One of the major disadvantages of MMSE is its dependence on the estimated SNR along with the channel state information (CSI) and the requirements of power allocation among the users (UEs). This leads to an increase in complexity and high power consumption. To get rid of the dependency on the estimated SNR, a fixed real-valued regularized parameter is introduced (RZF algorithm) [10,11]. The transmission power efficiency can be further improved by considering a complex regularization factor. As reported in [12], the authors have proposed a complex regularized ZF (CRZF) scheme and analyzed its performance. As in [12], it has the same computational complexity as a conventional ZF scheme. In this paper, the authors have modified the CRZF algorithm in order to reduce the complexity with improved system performance.

Lots of efforts have been imparted for designing the HPs. Apart from ZF and MMSE, the maximum ratio transmission (MRT) scheme is well investigated [13]. Over the years there are many proposal for designing efficient HPs such as Kalman filter based approach [14], block diagonalization scheme [15], modified block diagonalization scheme [16], singular-value-decomposition (SVD) based approach [17], and lattice reduction (LR) based approach [18–21]. To boost the performance of the mMIMO system, the authors in [22] have proposed a framework for LR-aided precoding in Vector perturbation (VP). Here, the authors have examined the possibility of exploiting the LR-ZF and LR-successive interference cancellation (SIC), and approximate message passing (AMP) algorithm to improve the symbol error rate (SER) performance of the mMIMO system with reduced complexity. In the case of mMIMO, the complexity of the system is a big concern, and to design low-complex HPs artificial Neural Network/deep learning (DL) based algorithms are proposed and extensively studied. In [23], a deep neural network (DNN) based HP framework is proposed for reducing the SER and improving SE of a mmWave-mMIMO system. Further, the authors [24] have proposed an effective convolutional neural network (CNN) framework for the joint design of precoder and combiners.

Now the increase in complexity in HP due to the matrix inversion process puts a severe question on its realization for the mMIMO system. Some efforts have been endeavored to reduce the complexity of the precoders. In this regard, truncated polynomial expansion (TPE) [25] and Neumann series (NS) precodings [26] are proposed and well investigated. The NS precoder is beneficial with a small number of iterations. However, in the case of a large number of iterations, it exhibits the same order of complexity as for ZF. Further to decrease the computational complexity Jacobi iteration-based precoder [27], Gauss–Seidel (GS) precoding [28], successive over-relaxation (SOR) precoding [29], symmetric SOR (SSOR) precoding [30], weighted SSOR (WSSOR) precoding [31] and modified SOR (MSOR) [32] are proposed and evaluated. These methods are effective to convert the matrix inversion into a linear equation through an iterative approach and can provide a near-optimal performance of ZF.

This motivates the authors to utilize the SSOR algorithm to reduce the complexity of the CRZF precoder and thereby improving the performance of the mmWave-mMIMO-NOMA system. In this paper, the authors have proposed a sub-connected SSOR-CRZF precoder for the mmWave-mMIMO-NOMA system. This paper presents a comparative analysis between the proposed SSOR-CRZF and MRT, ZF, RZF, TPE, SSOR, and CRZF

precoders. The performances have been analyzed in terms of SE, EE, and computational complexity. The proposed SSOR-SRZF precoder exhibits better performance in comparison to MRT, ZF, RZF, TPE, and SSOR precoders. Whereas it provides a marginal improvement against the CRZF with reduced computational complexity.

This paper provides an assessment of the effectiveness of the SSOR-CRZF precoder for enhancing the SS and EE of the mmWave-mMIMO-NOMA system with reduced complexity in comparison to the ZF precoder. The main contribution of this work can be briefly summarized as follows

- In a mMIMO system, reduction in the computational complexity is an important aspect. In this paper, the authors have proposed a SSOR-CRZF procoder to improve the mMIMO-NOMA system performance.
- The performance of the proposed SSOR-CRZF precoder is compared with MRT, ZF, RZF, TPE, SSOR, CRZF precoders in terms of SE, EE, and computational complexity.
- Demonstrate that the proposed algorithm significantly enhances the system performance than the conventional linear precoders.
- Demonstrate that the proposed algorithm improves the system performance marginally in comparison with the CRZF algorithm and provides additional benefits of low computational complexity.

The rest of this paper is structured as follows. In Section 2, a system model is presented. Section 3 represents the complexity comparison between the proposed and conventional precoders. In Section 4, various algorithms are evaluated through the simulation and comparative analysis has been carried out. The conclusion is given in Section 5.

Notations: $\mathbb{C}$ denotes the complex field. $\mathbb{E}[\cdot]$ denotes the expectation. $\|\cdot\|_2$ denotes the l_2 vector norm. $|\cdot|$ is used for absolute value. Here, $\left[\mathbf{F}^{rf}\right]_i$, $\left[\mathbf{F}^{rf}\right]_{:,j}$ and $\left[\mathbf{F}^{rf}\right]_{i,j}$ denote the ith row, the jth column, and the entry in the ith row and the jth column of $\mathbf{F}^{rf}$, respectively. Here, $\mathbf{h}^T$, $\mathbf{h}^H$, and $\mathbf{h}^{-1}$ denote the transpose, Hermitian transpose and inverse of $\mathbf{h}$. All the necessary acronyms are defined in Table 1.

Table 1. List of acronyms and corresponding definitions.

Acronym	Definition
mmWave	Millimeter-wave
mMIMO	Massive Multiple-Input Multiple-Output
NOMA	Non-Orthogonal Multiple Access
SE	Spectral Efficiency
EE	Energy Efficiency
HP	Hybrid Precoder
ZF	Zero-Forcing
MMSE	Minimum Mean Squared Error
MRT	Maximum Ratio Transmission
RZF	Regularized Zero-Forcing
CRZF	Complex Regularized Zero-Forcing
CSI	Channel State Information
SNR	Signal to Noise Ratio
SINR	Signal to Interference Plus Noise Ratio
SVD	Singular-Value-Decomposition
LR	Lattice Reduction
VP	Vector Perturbation
SIC	Successive Interference Cancellation
AMP	Approximate Message Passing
TPE	Truncated Polynomial Expansion
NS	Neumann Series
GS	Gauss–Seidel
SOR	Successive Over-Relaxation
SSOR	Symmetric Successive Over-Relaxation
WSSOR	Weighted SSOR
MSOR	Modified SOR
BS	Base Station

Table 1. *Cont.*

Acronym	Definition
UE	User Equipment
FC	Fully Connected Structure
SC	Sub-connected Structure
AOD	Angle of Departure

2. System Model

In this paper, the authors have considered a multiuser mmWave-MIMO-NOMA system under a downlink scenario as in Figure 1. All the necessary symbols for mathematical formulation are presented in Table 2. Here the base station (BS) is equipped with N_t transmit antennas. In this paper, N^{rf} RF chains are used to support K single antenna UEs [33,34]. The proposed system supports the users by exploiting the spatial diversity with $N^{rf} \leq K < N_t$. Here, the sub-connected (SC) structure is proposed for the mmWave-MIMO system. We also assume that $(M = N_t/N^{rf})$ M antennas are connected to each RF chains. In HP, B^n, the number of beams produced cannot exceed N^{rf} [33]. In this paper, it is assumed that $B^n = N^{rf}$. In the case of an HP-aided MIMO system, each beam can be utilized to support a single user but, by exploiting NOMA, each beam can support multiple users. Thus, for such a system, the K UEs can be supported through B^n clusters corresponding to the number of beams.

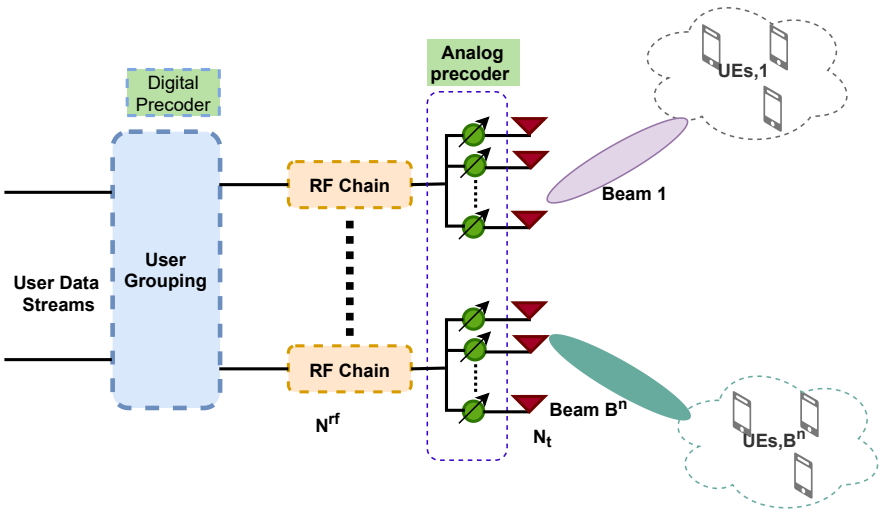

Figure 1. The system model for HP-aided mmWave mMIMO-NOMA with sub-connected architecture.

Table 2. List of symbols and corresponding definitions.

Symbol	Definition
N_t	Transmit antennas at BS.
N^{rf}	Number of RF Chains.
M	Number of antennas per RF chain.
K	Number of Users.
B^n	Number of Beam.
$\mathbf{f}_b^{BB}$	Base-band Digital Precoder.
$\mathbf{F}_{rf}$	RF Precoder.
B	Number of Bits for representing Quantization Level.
$y_{b,k}$	Received baseband signal corresponding to Kth UE in bth beam.
$\mathbf{h}_{b,k}$	Channel matrix corresponding to Kth UE in bth beam.
$\beta_{b,k}^{(l)}$	Complex gain of the lth path for the kth UE in the bth beam.
$\theta_{b,k}^{l}$	Azimuth angle of AOD of the lth path for the kth UE in the bth beam.
$\phi_{b,k}^{l}$	Elevation angleof AOD of the lth path for the kth UE in the bth beam.
$\mathbf{a}(\theta)$	Array response corresponding to N_t no. of altenna elements.
P	Power Allocation Matrix.
S	Transmitter signal vector.

Table 2. *Cont.*

Symbol	Definition
$\gamma_{b,k}$	SINR corresponding to the kth UE in the bth beam.
$R_{b,k}$	Achievable rate at the kth user in the bth beam.
R_{sum}	Achievable sum rate of the system.

In this structure the UEs data streams are passed through the baseband digital precoder $\mathbf{f}_b^{BB}\left[N^{rf}\times 1\right]$, $b\in[1,B^n]$ for the bth beam. Before transmission, $N_t\times N^{rf}$ RF precoder ($\mathbf{F}^{rf}$) is implemented by exploiting analog phase shifter. Here, it is considered that each elements are subjected to the condition to satisfy $\left(\left[\mathbf{F}^{rf}\right]_{:,j}\left[\mathbf{F}^{rf}\right]_{:,j}^{H}\right)_{l,l}=N_t^{-1}$ with the constant modulus constraint of $\left|\left[\mathbf{F}^{rf}\right]_{i,j}\right|=N_t^{-1/2}, 1\le i\le N_t, 1\le j\le N^{rf}$ and quantized phases: $\left[\mathbf{F}^{rf}\right]_{i,j}=(N_t)^{-1/2}exp\left(j[\Theta]_{i,j}\right)$. Here, the phase $[\Theta]_{i,j}$ is quantized as $[\Theta]_{i,j}\in :=\left\{\frac{2\pi n}{2^B}: n=0,\ldots,2^B-1\right\}$. Additionally, the total power constraint is realized by having normalized $\mathbf{f}_b^{BB}, b=1,\ldots,B^n$ for the bth beam so that $\left\|\mathbf{F}^{rf}f_b^{BB}\right\|_2=1$ for $b=1,\ldots,B^n$. Using NOMA, it is established that each beam can support multiple users. Let S_b for $b=1,\ldots,B^n$ denote the set of users served by the bth beam with $|S_b|\ge 1$, and $S_i\cap S_j=\Phi$ for $i\ne j$. Furthermore, also it is considered, $\sum_{b=1}^{B^n}|S_b|=K$.

Let us consider that $s_{b,k}$ $(\mathbb{E}[|s_{b,k}|^2]=1)$ be the transmitted signal towards the kth UE through the bth beam. As a part of the NOMA transmission protocol, BS utilized superposition coding for the successful transmission of multiple users information simultaneously. It is worth noting that the total power P is distributed equally over all the K UEs. Successive interference cancellation (SIC) is used at the receiver side to extract the information.

The received baseband signal $y_{b,k}$ at the kth UE in the bth beam $[k=1,\ldots,|S_b|]$ is written as

$$y_{b,k}=\mathbf{h}_{b,k}^H\mathbf{F}^{rf}\sum_{i=1}^{B^n}\sum_{j=1}^{|S_i|}\mathbf{f}_i^{BB}\sqrt{p_{i,j}}s_{i,j}+n_{b,k}. \tag{1}$$

$$\begin{aligned}&\underbrace{=\mathbf{h}_{b,k}^H\mathbf{F}^{rf}\mathbf{f}_b^{BB}\sqrt{p_b}s_{b,k}}_{\text{Desired signal}}\\ &\underbrace{+\mathbf{h}_{b,k}^H\mathbf{F}^{rf}\mathbf{f}_b^{BB}\left(\sum_{j=1}^{k-1}\sqrt{p_{b,j}}s_{b,j}+\sum_{j=k+1}^{|S_b|}\sqrt{p_{b,j}}s_{b,j}\right)}_{\text{Intra-beam Interference}}\\ &\underbrace{+\mathbf{h}_{b,k}^H\mathbf{F}^{rf}\sum_{i\ne b}\sum_{j=1}^{|S_i|}\mathbf{f}_i^{BB}\sqrt{p_{i,j}}s_{i,j}}_{\text{Inter-beam Interference}}\underbrace{+n_{b,k}}_{\text{Noise Signal}},\\ &=\mathbf{h}_{b,k}^H\mathbf{F}^{rf}\mathbf{F}^{BB}\mathbf{P}\mathbf{s}+n_{b,k},\end{aligned} \tag{2}$$

where $\mathbf{F}^{RF}\in\mathbb{C}^{N_t\times N^{rf}}$ is the analog precoder matrix, $\mathbf{F}^{BB}=[\mathbf{f}_1^{BB},\ldots,\mathbf{f}_{B^n}^{BB}]\in\mathbb{C}^{N^{rf}\times B^n}$ is the digital precoder matrix, $\mathbf{h}_{b,k}\in\mathbb{C}^{N_t\times 1}$ is the channel vector, $\mathbf{P}=diag\{\mathbf{p}_1,\ldots,\mathbf{p}_{B^n}\}$ corresponding to the power allocation matrix, the transmitted signal vector is represented by $\mathbf{s}=\left[s_{1,1},\ldots,s_{1,|S_b|},\ldots,s_{B^n,1},\ldots,s_{B^n,|S_b|}\right]^T\in\mathbb{C}^{K\times 1}$, $p_{b,k}$ denotes the transmit power for the kth UE in the bth beam, and $n_{b,k}\sim\mathcal{CN}(0,\sigma_n^2)$ represents the additive white Gaussian noise (AWGN) with zero mean and σ_n^2 variance added at the kth UE in the bth beam. At the UE end, SIC will be utilized to detect the interference free signal.

2.1. Channel Model

The millimeter-wave channel can be characterized by high path loss in free space, limited spatial selectivity, and a highly correlated channel. This paper adopts the geometric extended Saleh-Valenzuela model [35]. The channel matrix $\mathbf{h}_{b,k}$ corresponding to kth UE in the bth beam can be expressed as

$$\mathbf{h}_{b,k} = \sqrt{\frac{N_t}{\mathcal{L}_{b,k}}} \sum_{l=1}^{\mathcal{L}_{b,k}} \beta_{b,k}^{(l)} \mathbf{a}_R\left(\theta_{b,k}^l, \phi_{b,k}^l\right) \mathbf{a}_T\left(\theta_{b,k}^l, \phi_{b,k}^l\right). \tag{3}$$

where $\beta_{b,k}^{(l)}$ is the complex gain of the lth path for the kth UE in the bth beam. It is considered to be with complex Gaussian zero mean and unity variance. Here, $\theta_{b,k}^l$ and $\phi_{b,k}^l$ represent the azimuth and elevation angle of departure (AOD) of the $l$thpath. Here $\mathbf{a}_R\left(\theta_{b,k}^l, \phi_{b,k}^l\right)$ and $\mathbf{a}_T\left(\theta_{b,k}^l, \phi_{b,k}^l\right)$ represent normalized receive and transmit array response vectors. Assuming an uniform linear array (ULA) with N_t number of elements, the array response vector $\mathbf{a}(\theta)$ can be expressed as

$$\mathbf{a}(\theta) = \frac{1}{\sqrt{N_t}}\left(1, e^{j\varrho d\, sin(\theta)}, \ldots, e^{j(N_t-1)\varrho d\, sin(\theta)}\right)^T. \tag{4}$$

2.2. Sum Rate

Here it is considered that the inter-element distance $d = \lambda/2$ and $\varrho = 2\pi/\lambda$. As the array responds in elevation, the direction is invariant, therefore, ϕ is not considered in Equation (4). It is also assumed that both the BS and UEs have the perfect and instantaneous CSI and also the receivers are perfectly synchronized w.r.t time and frequency.

As mentioned, in this mmWave-mMIMO-NOMA system, at the receiver side SIC is performed to extract the desired information. That means by exploiting SIC, the kth user in the bth beam can effectively cancel out the interference from the dth user ($\forall j > b$). Therefore, the received signal at the kth user in the bth beam can be expressed as

$$\begin{aligned} \hat{y}_{b,k} = \bar{\mathbf{h}}_{b,k}^H \mathbf{f}_b^{BB} \sqrt{p_{b,k}} s_{b,k} + \bar{\mathbf{h}}_{b,k}^H \mathbf{f}_b^{BB} \sum_{j=1}^{k-1} \sqrt{p_{b,j}} s_{b,j} \\ + \bar{\mathbf{h}}_{b,k}^H \sum_{i \neq b} \sum_{j=1}^{S_i} \mathbf{f}_i^{BB} \sqrt{p_{i,j}} s_{i,j} + n_{b,k}, \end{aligned} \tag{5}$$

where the effective channel vectors is denoted by $\bar{\mathbf{h}}_{b,k}^H (= \mathbf{h}_{b,k}^H \mathbf{F}^{rf})$ Accordingly the signal to interference plus noise ratio (SINR) ($\gamma_{b,k}$) for the kth UE in the bth beam can be expressed as

$$\gamma_{b,k} = \frac{\left\| \bar{\mathbf{h}}_{b,k}^H \mathbf{f}_b^{BB} \right\|_2^2 p_{b,k}}{\zeta_{b,k}}, \tag{6}$$

where

$$\zeta_{b,k} = \left\| \bar{\mathbf{h}}_{b,k}^H \mathbf{f}_b^{BB} \right\|_2^2 \sum_{j=1}^{k-1} p_{b,j} + \sum_{i \neq b} \left\| \bar{\mathbf{h}}_{b,k}^H \mathbf{f}_b^{BB} \right\|_2^2 \sum_{j=1}^{|S_i|} p_{i,j} \sigma_n^2. \tag{7}$$

Therefore, the achievable rate at the kth user in the bth beam is

$$R_{b,k} = log_2(1 + \gamma_{b,k}). \tag{8}$$

The achievable sum rate of the system is given by

$$R_{sum} = \sum_{b=1}^{B^n} \sum_{k=1}^{|S_b|} R_{b,k}. \tag{9}$$

The sum rate can be improved by suitable design analog and digital precoder.

2.3. User Grouping

In this system, the number of UEs served (K) is greater than the N^{rf}, $B^n = N^{rf}$ and channel matrix $\mathbf{H} = [\mathbf{h}_1, \ldots, \mathbf{h}_K]$. Thus, it is required to allocate K UEs into B^n groups. To serve the users, this paper considered the modified K-Means user grouping algorithm for the proposed mmWave-NOMA system. Based on the normalized channel correlation among user channels, the algorithm forms user groups. At the initial stage, one representative UE is selected corresponding to each beam by minimizing the normalized channel correlation among the beam selected representatives. To minimize the inter beam interference, UEs are grouped into different beams based on the channel correlation. The modified K-Means algorithm [34] is presented in Algorithm 1. In traditional K-means user grouping algorithm [33], the cluster heads are selected randomly. The distinct advantage of Algorithm 1 is basically its selection criterion for the cluster heads (Step 10–15). In this algorithm, the optimal representative (Step 11) is chosen by considering the minimum channel correlation among the chosen representatives. Thereafter, the UEs that belong to highly correlated channels are assigned to the same beam to minimize intra-beam interference.

Algorithm 1 Modified K-Means User Grouping Algorithm

Input: $K(> N^{rf})$; B^n; Channel vector, $\mathbf{h}_k$ *for* $k \in (1, K)$; Initial correlation threshold $\delta(0 < \delta < 1)$

Output: Optimized user grouping $[\Gamma, \ldots, \Gamma_{B^n}]$

1 ***Initialize:*** $\Omega = \mathbf{0}^{B^n}$
2 $\mathcal{K} = [1, \ldots, K]$
3 $\acute{\mathbf{h}} = [\|\mathbf{h}_1\|_2, \ldots, \|\mathbf{h}_K\|_2]$; channel gains for each user
4 $\bar{\mathbf{h}} = [\frac{\mathbf{h}_1}{\|\mathbf{h}_1\|_2}, \ldots, \frac{\mathbf{h}_K}{\|\mathbf{h}_K\|_2}]$; Normalized channel gains for each user
5 $[\sim, \mathcal{D}] = sort(\boldsymbol{h}', 'descend')$
6 $\Omega(1) = \mathcal{D}(1)$
7 $\mathcal{D}(1) = []$; Remove the 1st element of $\mathcal{D}$
8 $\Xi = \mathcal{D}$ Rrmaining user set
9 b=2
10 **while** $b \leq B^n$ **do**
11 $\quad \mathbf{w} = \left|\bar{\mathbf{h}}_i^H \bar{\mathbf{h}}_j\right|, i \in \Xi, \forall j \in \Omega$
12 $\quad [\sim, \acute{\mathcal{D}}] = min(find(\mathbf{w} < \delta))$
13 $\quad \Omega(b) = \Xi(\acute{\mathcal{D}}(1))$; Merge new cluster head to Ω
14 $\quad \mathcal{D}(find(\mathcal{D} == \Omega(b))) = [\,]$; Remove $\Omega(b)$ from $\mathcal{D}$
15 $\quad$ b=b+1
16 $\Omega = \Omega_1, \ldots, \Omega_{B^n}$ with $\Omega_b = k_b \in \mathcal{K}$, Cluster heads selected in **step 12**
17 f = 1;
18 **while** $\Omega_b^f \neq \Omega_b^{f-1}$ **do**
19 $\quad$ Set $(\Gamma_b)_{b=1}^{B^n} = (\Omega_b^f)_{b=1}^{B^n}$
20 $\quad$ **for** $k = \mathcal{K}/\Omega_b^f$ **do**
21 $\quad\quad b^* = arg\ \max_{1 \leq b \leq B^n} Corr_{k,\Omega_b^f}$
22 $\quad\quad \Gamma_{b^*} = \Gamma_{b^*} \bigcup k$
23 $\quad$ f = f + 1
24 $\quad$ Update Ω_b^f

On the other hand, the UEs belonging to low correlated channels are assigned to different beams to minimize inter-beam interference.

2.4. Hybrid Analog-Digital Precoder

The main aim of this paper is to maximize the sum-rate [as in (9)] by jointly solving the power allocation, digital and analog RF precoder optimizing problem. The problem statement can be expressed as

$$\max_{p_{b,k},\, \mathbf{f}_b^{BB},\, \mathbf{F}^{rf}} R_{sum} \left(R_{sum} = \sum_{b=1}^{B^n} \sum_{k=1}^{|S_b|} R_{b,k} \right) \tag{10a}$$

$$s.t. R_{b,k} \geq R_{b,k}^{min},\ \forall b,k, \tag{10b}$$

$$p_{b,k} \geq 0,\ \forall b,k, \tag{10c}$$

$$\sum_{b=1}^{B^n} \sum_{k=1}^{|S_b|} p_{b,k} \leq P, \tag{10d}$$

$$\left| \mathbf{F}_{i,j}^{rf} \right|^2 = \frac{1}{N_t}, 1 \leq i \leq N, 1 \leq j \leq N^{rf}, \tag{10e}$$

$$\left\| \mathbf{F}^{rf} \mathbf{f}_b^{BB} \right\|_2 = 1\ \forall b, \tag{10f}$$

Here, the constraints (10b) ensures that the kth user in the bth beam must attain the minimum desirable data rate. The constraints (10c) and (10d) represent that the power transmitted by the BS for each UE must be positive and total power can not exceed the limit P (transmitted power constraint). In the case of analog precoder, the non-zero elements in the precoding matrices are realized by the phase shifter and it satisfies the constant-modulus constraint as in (10e). The constraint (10f) represents the unit power constraint for the HP matrix. Looking at (10f), it can be seen that an optimized digital precoder for each beam is required. As the optimization problem turns out to be a non-convex optimization problem, therefore it is difficult to obtain a globally optimal solution.

The channel capacity of the UEs can be improved by reducing inter-beam interference and also by improving the effective channel gain. The HP scheme is capable to achieve the full potential of the mmWave-mMIMO system with reduced hardware constraints. Motivated by the works presented in [33,34,36], it is considered to discuss the analog RF precoder and digital baseband precoder separately. The authors have implemented an efficient analog RF precoding algorithm (for $\mathbf{F}^{rf}$) as in [34]. In this paper, the authors have proposed a low-dimensional digital baseband precoding algorithm (for $\mathbf{F}^{BB}$) and compared its performance with existing digital precoders.

2.4.1. Analog Precoder

The main motive of the analog precoder is to orient the phases of $\mathbf{H} = [\mathbf{h}_1, \ldots, \mathbf{h}_K]$ to produce a large array gain by exploiting a large number of antennas in mMIMO system. The analog precoding algorithm is presented in Algorithm 2. As in [33], quantized phase shifters are used for the analog precoder. In this paper, the authors have considered both FC and SC structures. The non-zero elements corresponding to the FC analog precoder ($\mathbf{AP}^{full}$) matrix belong to

$$\left\{ \frac{1}{\sqrt{N_t}} exp(j\frac{2\pi n}{2^B}) : n = 0, 1, \ldots, 2^B - 1 \right\}. \tag{11}$$

Similarly, for SC structure, the non-zero elements corresponding to the analog precoder ($\mathbf{AP}^{sub}$) matrix belong to

$$\left\{ \frac{1}{\sqrt{M}} exp(j\frac{2\pi n}{2^B}) : n = 0, 1, \ldots, 2^B - 1 \right\}. \tag{12}$$

The analog precoding matrix ($\mathbf{AP}^{full}/(\mathbf{AP}^{sub})$) can be designed by maximizing the array gain. In other words, analog precoding matrix can be obtained by considering the channel matrix corresponding to users in cluster (Γ_{B^n}). Therefore, the array gain for FC and SC structure can be expressed as $\left|\bar{\mathbf{H}}^H \bar{\mathbf{ap}}_b^{full}\right|^2$ and $\left|\bar{\mathbf{H}}^H \bar{\mathbf{ap}}_b^{sub}\right|^2$, respectively. Here, $\bar{\mathbf{H}}$ represents the aggregate downlink channel from the BS to UEs corresponding to bth beam. Thus, the analog precoding matrix for FC structure can be expressed as,

$$\bar{\mathbf{ap}}_b^{full}(m) = \frac{1}{\sqrt{N_t}} exp(j\frac{2\pi\theta}{2^B}), \tag{13}$$

where

$$\theta = \underset{n \in 0,1,\ldots,2^B-1}{arg\,min} \left|\Theta(m) - \frac{2\pi n}{2^B}\right|. \tag{14}$$

Here, $\Theta = \angle\bar{\mathbf{H}}$, is the phases corresponding to the aggregated channel matrix $\bar{H}$ and $m = 1, 2, \ldots, N_t$. Similarly, for SC structure, the analog precoding matrix can be expressed as,

$$\bar{\mathbf{ap}}_b^{sub}(m) = \frac{1}{\sqrt{M}} exp(j\frac{2\pi\theta}{2^B}), \tag{15}$$

where $m = (b-1)M + 1, (b-1)M + 2, \ldots, gM$, and θ as in (14).

Algorithm 2 Analog Precoder

Input: $K(> N^{rf})$;N^{rf}; $\mathbf{H} = [\mathbf{h}_1, \ldots, \mathbf{h}_K]$; $\Gamma_1, \ldots, \Gamma_{B^n}$;$N_t$
Output: $\mathbf{F}^{rf}$

Initialize: $\mathbf{F}^{rf} = \mathbf{0}^{N_t \times N^{rf}}$; No. of Quantization Bits B
$\hat{\theta} = \frac{2\pi n}{2^B}; n = 0, 1, \ldots, 2^{B-1}$; Phase set
for $b = 1 : N^{rf}$ **do**
  $\bar{\mathbf{H}} = [\mathbf{H}]_{:,\Gamma_b}$
  $\Theta = \angle\bar{\mathbf{H}}$; Phases corresponding to the aggregated channel matrix $\bar{\mathbf{H}}$
  $\theta = \mathbf{0}^{N_t}$
  for $m = 1 : N_t$ **do**
    $[\sim, q] = min\left|[\Theta]_m - \hat{\theta}\right|$
    $\theta(m) = \left[\hat{\theta}\right]_q$
  $\mathbf{F}^{rf}(:, b) = \frac{1}{\sqrt{N_t}} exp(j * \frac{2\pi\theta}{2^B})$

The Algorithm 2 is addressing the analog precoder for FC structure ($\mathbf{F}^{rf} = \mathbf{AP}^{full}$). The same can be extended for SC structure ($\mathbf{F}^{rf} = \mathbf{AP}^{sub}$) with the necessary changes for implementing Equation (15). The combination of analog and digital precoder maximize the achievable sum rate by mitigating the interference.

2.4.2. Digital Precoder

A brief review related to the commonly used linear precoders is discussed. According to [11], the conventional ZF precoding ($\mathbf{F}_{ZF}^{BB}$) matrix can be expressed as

$$\mathbf{F}_{ZF}^{BB} = \beta_{ZF}\mathbf{H}^H(\mathbf{H}\mathbf{H}^H)^{-1}, \tag{16}$$

where, β_{ZF} denotes the power normalization factor that can be defined as $\beta_{ZF} = \sqrt{\frac{K}{tr(\mathbf{H}\mathbf{H}^H)^{-1}}}$.

Similarly, for RZF the precoding matrix can be expressed as

$$\mathbf{F}_{RZF}^{BB} = \beta_{RZF}\mathbf{H}^H(\mathbf{H}\mathbf{H}^H + \hat{\alpha}\mathbf{I})^{-1}, \tag{17}$$

where $\hat{\alpha}$ is the regularization parameter and it is predefined during the transmission. $\mathbf{I}$ is a $N^{rf} \times K$ identity matrix and its dimension is chosen in accordance with the hybrid precoder design as in this paper. As in [11], RZF precoder is independent of the power allocation to the UEs and also this precoder maintains a constant value of $\hat{\alpha}$, regardless of any changes in the noise power σ_n^2. As in Equations (16) and (17), the precoders requires the matrix inversion and therefore the complexity is of the order of $\mathcal{O}(K^3)$.

Recently in [12], authors have proposed CRZF precoding scheme to enhance the system performance. The precoding matrix for CRZF can be expressed as

$$\mathbf{F}_{CRZF}^{BB} = \beta_{CRZF}\mathbf{H}^H(\mathbf{H}\mathbf{H}^H + \alpha\mathbf{I})^{-1}, \tag{18}$$

where α is a complex valued regularization parameter and it is due to the complex nature of the AWGN. As in [12], α can be estimated from the covariance matrix of the AWGN and can be expressed as $\mathbf{R}_{\eta}^{-1}/\gamma \triangleq \alpha\mathbf{I}$. In this context, $\mathbf{R}_{\eta}^{-1}$ can be expressed as $\mathbf{R}_{\eta}^{-1} = \mathbb{E}[\boldsymbol{\eta}\boldsymbol{\eta}^H] = \mathbb{E}(\boldsymbol{\eta}_{real} + j\boldsymbol{\eta}_{imag})(\boldsymbol{\eta}_{real} + j\boldsymbol{\eta}_{imag})^H$ and $\beta_{CRZF} = \gamma^{-1}$. As $\aleph$ is a complex term and can be expressed as $\alpha = \alpha_r + j\alpha_{im}$. Here, $\alpha_r \triangleq \mathbb{E}[\boldsymbol{\eta}_{real}\boldsymbol{\eta}_{real}^H + \boldsymbol{\eta}_{imag}\boldsymbol{\eta}_{imag}^H]$ and $\alpha_{im} \triangleq \mathbb{E}[\boldsymbol{\eta}_{imag}\boldsymbol{\eta}_{real}^H - \boldsymbol{\eta}_{real}\boldsymbol{\eta}_{imag}^H]$. Therefore, it is very clear that for $\alpha_{im} = 0$, the regularization parameter is a real valued and the CRZF scheme reduces to the RZF.

Proposed Method (SSOR-CRZF): As investigated the CRZF significantly improves the system performance in comparison to conventional ZF and RZF precoders, however, like ZF and RZF, it also involves matrix inversion. In the case of the MIMO system, such computation becomes practically impossible to realize. In this paper, the authors have proposed an SSOR-CRZF digital precoder for the system as in Figure 1. The proposed Algorithm 3 utilizes the iterative SSOR method to form a CRZF matrix without any matrix inversion. In this proposed HP scheme, after the design of the analog precoder ($\mathbf{F}^{rf}$), a low-dimensional baseband digital (SSOR-CRZF) precoder is implemented considering the effective channel ($\breve{\mathbf{H}}$). As in Algorithm 3, the precoding algorithms begin with the calculation of the CRZF filtering matrix ($\mathbf{P}$) and it can be expressed as follows,

$$\mathbf{P} = \left(\breve{\mathbf{H}}\breve{\mathbf{H}}^H + \alpha\mathbf{I}_{N^{rf}\times N^{rf}}\right) \tag{19}$$

However, it is required to take the pseudo-inverse and this leads to an increase in the computational complexity. In order to reduce the complexity, authors in [30,32] have proposed SSOR-based precoding by exploiting the asymptotical orthogonality property of the wireless channel in massive MIMO. Now as in [30], for CRZF precoder, the transmitted signal ($\mathbf{x}$)

$$\mathbf{x} = \mathbf{F}_{CRZF}^{BB}\mathbf{s} = \beta_{CRZF}\mathbf{H}^H\left(\breve{\mathbf{H}}\breve{\mathbf{H}}^H + \alpha\mathbf{I}_{N^{rf}\times N^{rf}}\right)^{-1}\mathbf{s} = \beta_{CRZF}\breve{\mathbf{H}}^H\mathbf{P}^{-1}\mathbf{s} = \beta_{CRZF}\breve{\mathbf{H}}^H\mathbf{t}. \tag{20}$$

The main motivation of the SSOR method is to achieve the precoder matrix $\mathbf{t}$ without having any matrix inversion ($\mathbf{P}^{-1}$). As the initial step in the SSOR method, it decomposes the matrix $\mathbf{P}$ and can be expressed as $\mathbf{P} = \mathbf{D} + \mathbf{L} + \mathbf{L}^H$, where, $\mathbf{D}$, $\mathbf{L}$ and $\mathbf{L}^H$ represent the diagonal matrix, lower triangular matrix and the upper triangular matrix of $\mathbf{P}$, respectively. The iteration in the SSOR method can be carried out by utilizing the following steps:
step 1: Compute the forward first half iteration by

$$(\mathbf{D} + \omega\mathbf{L})\mathbf{t}^{(i+1/2)} = (1-\omega)\mathbf{D}\mathbf{t}^{(i)} - \omega\mathbf{L}^H\mathbf{t}^{(i)} + \omega\mathbf{s}, \tag{21}$$

step 2: Compute the reverse second half iteration by

$$(\mathbf{D} + \omega\mathbf{L})\mathbf{t}^{(i+1)} = (1-\omega)\mathbf{D}\mathbf{t}^{(i+1/2)} - \omega\mathbf{L}^H\mathbf{t}^{(i+1/2)} + \omega\mathbf{s}, \tag{22}$$

where i represents the number of iteration and ω is the relaxation parameter. As in [30], the optimal ω can be calculated by $\omega = 2/(1 + sqrt((1-a^2)))$ where $a = [1 + sqrt(Nr/Nt)]^2 - 1]$.

It is very clear that once the massive MIMO configuration is fixed the relaxation parameter ω also become fixed. The required vector $\mathbf{t}$ can be obtained after several iterations as mentioned in Equations (21) and (22). Thus, the desired precoding matrix cab be obtained by multiplying vector $\mathbf{t}$ with $\beta_{CRZF}\check{\mathbf{H}}^H$.Thus, it is clear that the computationally complex matrix inversion can be achieved through iterative methods.

Algorithm 3 Proposed Digital Precoder

Input: $K(> N^{rf})$; N^{rf}; $\mathbf{H} = [\mathbf{h}_1, \ldots, \mathbf{h}_K]$; $\Gamma = [\Gamma_1, \ldots, \Gamma_{B^n}]$; $\mathbf{F}^{rf}$;N_t;$B^n = N^{rf}$; α; N_iter

Output: $\mathbf{F}^{BB} = [\mathbf{f}_1^{BB}, \ldots, \mathbf{f}_{B^n}^{BB}] \in \mathbb{C}^{N^{rf} \times B^n}$ is the digital precoder matrix

1 ***Initialize:*** No. of Quantization Bits B

2 $\bar{\mathbf{H}} = \mathbf{H}^H\mathbf{F}^{rf}$

3 $\check{\mathbf{H}} \in \mathbb{C}^{N^{rf} \times N^{rf}} = [\bar{\mathbf{H}}_{\Gamma,1}]$

4 $\mathbf{P} = \left(\check{\mathbf{H}}\check{\mathbf{H}}^H + \alpha\mathbf{I}_{N^{rf} \times N^{rf}}\right)$; CRZF Filtering Matrix

5 $\mathbf{D} = diag(Diag(\mathbf{P}))$

6 $\mathbf{L} = -(tril(\mathbf{P}) - \mathbf{D})$

7 $\mathbf{U} = -(triu(\mathbf{P}) - \mathbf{D})$

8 $[Nr, Nt] = size(\mathbf{P})$

9 $a = [1 + sqrt(Nr/Nt)]^2 - 1$; $\omega = 2/(1 + sqrt((1 - a^2)))$; relaxation parameter

10 $Symbol = eye(Nr, Nr)$

11 $\mathbf{s}0 = zeros(Nr, length(Symbol))$

12 $i\_iter = 1$

13 $\mathbf{s}2 = \mathbf{s}0$;

14 **while** $i\_iter \leqslant N\_iter$ **do**

15 $\quad \mathbf{s}0 = \mathbf{s}2$

16 $\quad \mathbf{s}1 = (D - \omega * L)^{-1} * (\omega * Symbol + ((1 - \omega) * D + \omega * U) * \mathbf{s}0)$

17 $\quad \mathbf{s}2 = (D - \omega * U)^{-1} * (\omega * Symbol + ((1 - \omega) * D + \omega * L) * \mathbf{s}1)$

18 $\quad i\_iter = i\_iter + 1$

19 $\hat{\mathbf{F}}^{BB} = \check{\mathbf{H}} * s2$

20 $\hat{\mathbf{F}}^{BB} = [\hat{\mathbf{f}}_1^{BB}./\mathbf{f}_1^{BB^*}, \ldots, \hat{\mathbf{f}}_{N^{rf}}^{BB}./\mathbf{f}_{N^{rf}}^{BB^*}]$./ denote element-wise dot operator and $\mathbf{F}^{BB^*} = [\mathbf{f}_1^{BB^*}, \ldots, \mathbf{f}_{N^{rf}}^{BB^*}]$; where, $\mathbf{f}_n^{BB^*} = repmat(\left\|\mathbf{F}^{rf}\hat{\mathbf{f}}_n^{BB}, N^{rf}, 1\right\|_2), n = 1, \ldots, N^{rf}$

21 $\mathbf{F}^{BB} = \mathbf{0}^{N^{rf} \times K}$

22 $[\mathbf{F}^{BB}]_{:,[\Gamma]:,1} = \hat{\mathbf{F}}^{BB}$

23 **for** $b = 1$ *to* N^{rf} **do**

24 $\quad \Xi = [\Gamma]_{b,:}$

25 $\quad \Xi = nonzeros(\Xi)^T$; discard the zero element

26 $\quad$ **for** $n = 2$ *to* $|\Xi|$ **do**

27 $\quad\quad [\mathbf{F}^{BB}]_{:,\Xi_n} = [\mathbf{F}^{BB}]_{:,[\Gamma]_{b,1}}$

In this paper, as a part of hybrid precoder design, analog RF precoder ($\mathbf{F}^{rf}$) is designed first and low dimensional digital precoder (SSOR-ZF) is implemented based on the effective channel matrix ($\bar{\mathbf{H}}$). Step 3 is for generating the CRZF filtering matrix and steps 5 to 19 are for the SSOR process to obtain the desired SSOR-CRZF precoder ($\hat{\mathbf{F}}^{BB}$). Finally, using steps 23 to 27, after N^{rf} iterations the base-band digital precoder ($\mathbf{F}^{BB}$) is designed.

3. Computational Complexity

In this section, the computational complexity of the SSOR-CRZF precoder and some existing precoders are analyzed [as in Table 3]. As in case of ZF, RZF, CRZF and SSOR-ZF, it is required to compute $\mathbf{H}\mathbf{H}^H$, and also it is possible to compute the complexity beyond $\mathbf{H}\mathbf{H}^H$.

Therfore, in case of ZF [as per Equation (16)], the computational complexity can be expressed as $\mathcal{O}(2(N^{rf})^3 + (N^{rf})^2)$. Similarly, for RZF [as per Equation (17)], the complexity can be expressed as $\mathcal{O}(2(N^{rf})^3 + 3(N^{rf})^2)$.

In the proposed precoder, $\mathbf{P} = \left(\check{\mathbf{H}}\check{\mathbf{H}}^H + \alpha \mathbf{I}_{N^{rf} \times N^{rf}}\right)$ and therefore, for SSOR-CRZF precoder, it can be written [from Equation (21)].

$$t_n^{i+1/2} = t_n^i + \frac{\omega}{p_{ii}}\left(s_i - \sum_{j=1}^{n-1} p_{nj} t_j^{n+1/2} + \sum_{j=n}^{N^{rf}} p_{nj} t_j^{(n)}\right), \tag{23}$$

where $P_{nn}(n = 1, \ldots, N^{rf})$ is the diagonal elements of $\mathbf{P}$ and the subscript n denotes the nth element in a vector. Equation (23) is basically responsible for the first section of the complexity and as in [32] the computational complexity is $i2(N^{rf})^2$ after i iterations. Furthermore the multiplication $\mathbf{H}^H\mathbf{t}$ required additional computational complexity of $(N^{rf})^2$. Furthermore, as the last section, multiplication with β_{CRZF} with $\mathbf{H}^H\mathbf{t}$ gives rise a computational complexity of (N^{rf}). Therefore, from the above analysis, it can be concluded that the overall computational complexity of the proposed SSOR-CRZF precoder in $\mathcal{O}(N^{rf} + (N^{rf})^2 + i2(N^{rf})^2)$.

Table 3. Computational complexity comparison.

Precoding Scheme	Computational Complexity
ZF	$\mathcal{O}(2(N^{rf})^3 + (N^{rf})^2)$
RZF	$\mathcal{O}(2(N^{rf})^3 + 3(N^{rf})^2)$
CRZF	$\mathcal{O}(2(N^{rf})^3 + 3(N^{rf})^2)$
SSOR-CRZF	$\mathcal{O}(N^{rf} + (N^{rf})^2 + i2(N^{rf})^2)$

4. Numerical and Simulation Results

To establish the superiority of the proposed SSOR-CRZF-aided hybrid precoding algorithm, this section presents the performance comparison of the proposed HP with the conventional ZF, RZF, MRT, TPE, SSOR, and CRZF precoders. Here in this work, a sub-connected (SC) structure for the hybrid precoding has been considered, and also it is considered that full/partial CSI information is available at the transmitter side. This section numerically evaluates the performance of the proposed HP in an mMIMO-NOMA system in terms of spectral efficiency, energy efficiency, and computational complexity of the proposed algorithm. As a part of the comparison, the authors have considered fully connected (FC), sub-connected structure (SC) of the precoding, and also fully digital (FD) system.

The simulation parameters are shown in Table 4. The MATLAB platform is used for the simulation. Here, the results are presented after taking an average of over 1000 random channel implementations.

Table 4. Simulation Parameters.

Parameters	Value
Base Station Antennas (N_t)	[16, 32, 48, 64, 96, 128]
User Terminals Antenna	1
Antenna array structure at BS	ULA with $\lambda/2$ antenna spacing
Number of RF chains (N^{rf})	4, 8
Transmitted Power	30 dB
Channel Model ($\mathbf{H}$)	Geometric Extended Saleh-Valenzuela model
Number of propagation paths per cluster (L)	10
Number of Users (K)	[4:12]
DOA/AOA phase quantization	B = [4, 2]
Hybrid Precoding Algorithms	MRT, ZF, RZF, TPE, SSOR,CRZF, SSOR-CRZF
Hybrid Precoding Structure	Fully Connected (FC) and Sub-connected Structure (SC)

4.1. Spectral Efficiency

Figure 2 represents the performance comparison between different precoders in terms of spectral efficiency as a function of SNR. The result under a mmWave mMIMO-NOMA system with $N_t = 16$ and $N^{rf} = 4$. As a part of the channel model, the authors have considered $K = 6$ users and $L = 10$ paths per user. The simulation results demonstrate that the proposed SSOR-CRZF performs much better than the other precoders like ZF, RZF, MRT, TPE, SSOR, and CRZF based on SC architecture. It is very much evident from the result that under SC structure SSOR-CRZF provides higher spectral efficiency at high SNR regions.

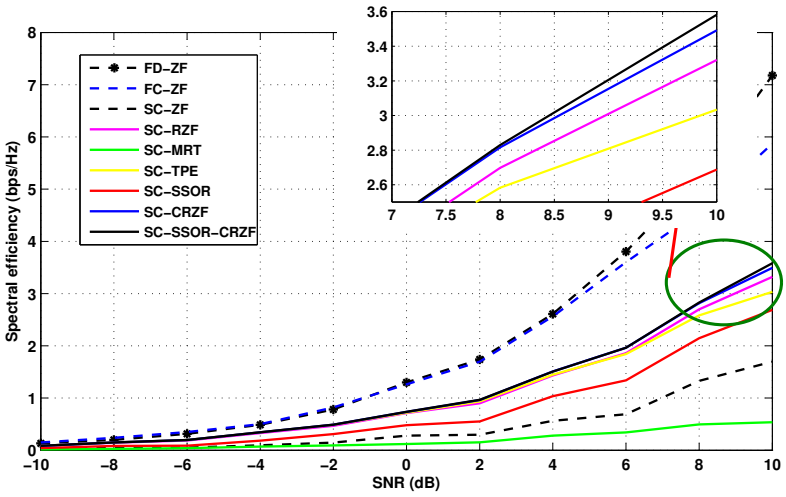

Figure 2. Spectral Efficiency Comparison.

Figure 3 represents the achievable spectral efficiency comparison with the change in N^{rf} . The result under a mmWave mMIMO-NOMA ULA system with $N_t = 32$. As a part of the channel model, the authors have considered $K = 10$ users and $L = 10$ paths per user. The impact of RF chains on the attainable spectral efficiency for $N^{rf} = [4, 8]$ is investigated. It is clearly visible that there is a significant gain in spectral efficiency with $N^{rf} = 8$ in comparison to $N^{rf} = 4$. For example, at SNR = 10 dB with $N^{rf} = 4$ and SSOR-CRZF precoder, the achievable spectral efficiency is 2.683 bps/Hz. Under the same condition, with $N^{rf} = 8$ the achievable spectral efficiency is 6.29 bps/Hz.

In this paper, the authors have evaluated the performance of the proposed low-resolution HPs for the mmWave-mMIMO-NOMA system. For this performance analysis, it is assumed that the mmWave-mMIMO-NOMA ULA system with $N_t = 32$ and $K = 10$ users. As a part of the HP design, it is assumed $N^{rf} = 4$ RF chains and digital PS as an element of an analog precoder with (2,4) bits resolution. The proposed SSOR-CRZF technique for 4-bit resolution manifests better performance compared with its counterparts as presented in Figure 4. It is very much evident that the system performance improves with the increase in the PS resolution but high-resolution PSs are not warranted as it is associated with additional cost and complexity.

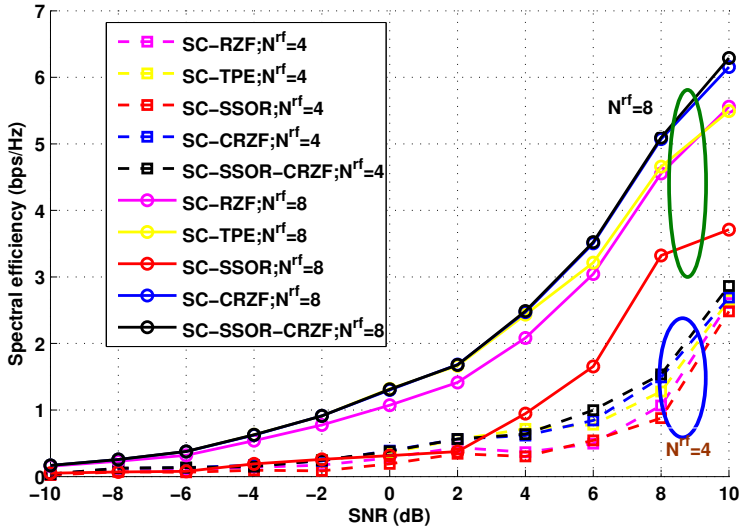

Figure 3. Spectral Efficiency Variation with N^{rf}.

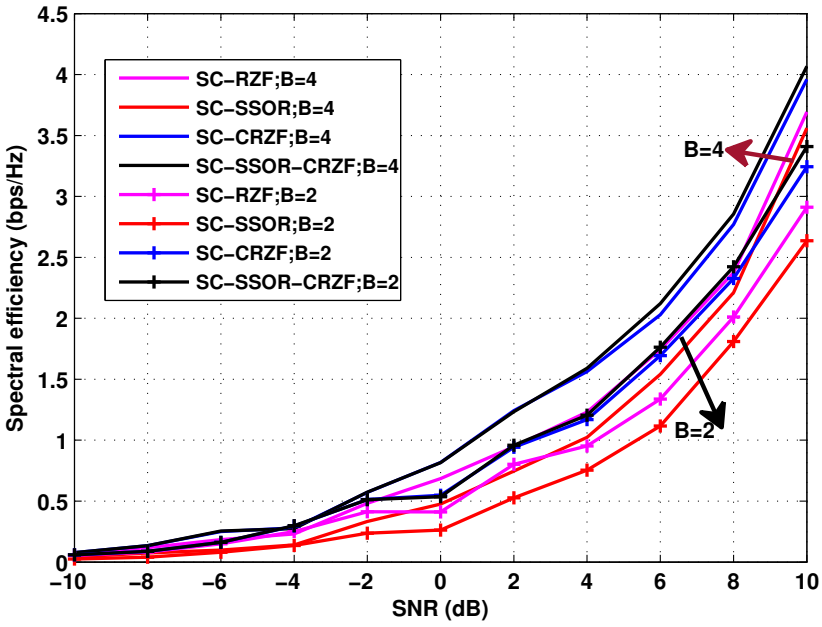

Figure 4. Spectral Efficiency Variation with B.

4.2. Energy Efficiency

In this section, the performance of mmWave-mMIMO-NOMA system is analysed in terms of energy efficiency (EE (bps/Hz/W)). As in [33], the EE can be expressed as $EE = \frac{R_{sum}}{P_t + N^{rf} P_{rf} + N_{ps} P_{ps} + P_{bb}}$, where, N_{ps} is the total number of phase shifters. In case of FC, $N_{ps} = N_t N^{rf}$ and for SC, $N_{ps} = N_t$. For this analysis, it is considered that the maximum transmitted power, P_t = 30 mW. It is considered to be the same for all precoder algorithms. The power is consumed by each RF chain, P_{rf} = 300 mW. For the simulation, the selected parameters, P_{ps} = 40 mW, P_{bb} = 200 mW.

Figure 5 shows the energy efficiency comparison between different precoders against the SNR variation. For this performance analysis, it is assumed that the mmWave mMIMO-NOMA system with $N_t = 16$. Furthermore, also $K = 6$ users and $L = 10$ paths per user. As a part of the HP design, it is considered that $N^{rf} = 4$ RF chains and digital PS is an element of an analog precoder with 4 bits resolution. As in the figure, it is very much obvious

that in the case of a fully digital (FD) system the EE is worst compared with others. This is because, in the FD system, the number of RF chains is equal to the number of base station antennas and it gives rise to energy consumption. On the contrary, the number of RF chains is much small in the case of an SC system. The SC-HPs are more energy-efficient than the FC-HPs as a less number of PS is utilized in the SC-HP. As in Figure 5, the proposed SSOR-CRZF outperforms the existing schemes under consideration in terms of energy efficiency. For example, at SNR = 10 dB the energy efficiency for the proposed SC-SSOR-CRZF, SC-CRZF, SC-SSOR, SC-TPE, SC-RZF, and SC-ZF are 1.702 bps/Hz/W, 1.687 bps/Hz/W, 1.299 bps/Hz/W, 1.466bps/Hz/W, 1.604 bps/Hz/W, and 0.8193 bps/Hz/W, respectively.

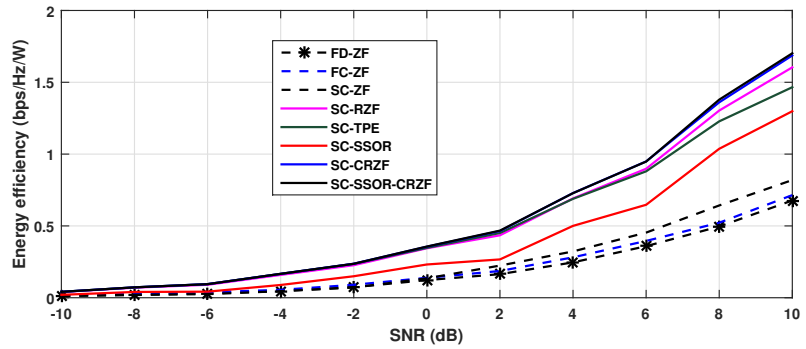

Figure 5. Energy Efficiency Comparison with SNR variation.

Figure 6 shows the energy efficiency comparison between different precoders against the variation in the number of users. For this analysis, SNR is kept at 10 dB. For this performance analysis, the mmWave-mMIMO-NOMA system with $N_t = 32$ is considered in this paper, and also $L = 10$ paths per user. As a part of the HP design, $N^{rf} = 4$ RF chains and digital PS as an element of an analog precoder with 4 bits resolution are considered. It is very much clear that even if the number of users is high, the EE of the SC-HPs is always higher than the other schemes.

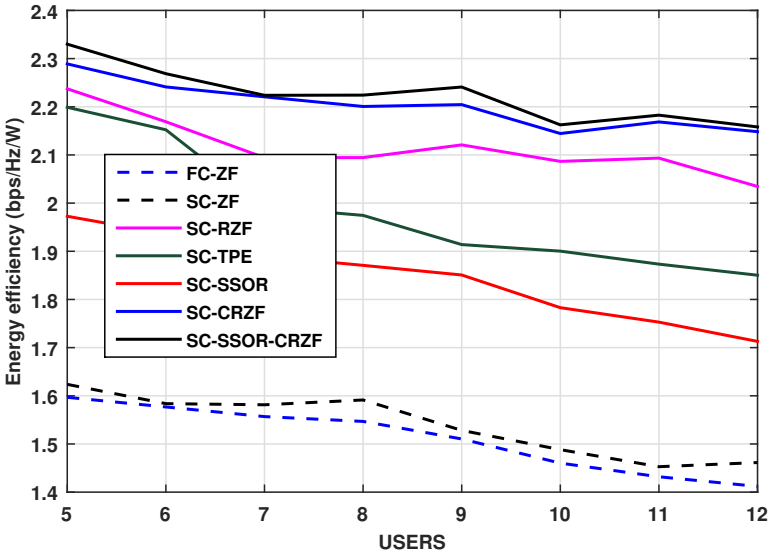

Figure 6. Energy Efficiency Variation with the No. of Users.

Figure 7 shows the energy efficiency comparison between difference precoders against the variation in the number of transmitting antennas (N_t). For this performance analysis, a mmWave-mMIMO-NOMA system with $K = 10$ users and $L = 10$ paths per user is considered. As a part of the HP design, we assume $N^{rf} = 8$ RF chains and digital PS as an

element of an analog precoder with 4 bits resolution. From Figure 7 there exists an optimal antenna array size to maximize the EE of the system under a fixed number of RF chains.

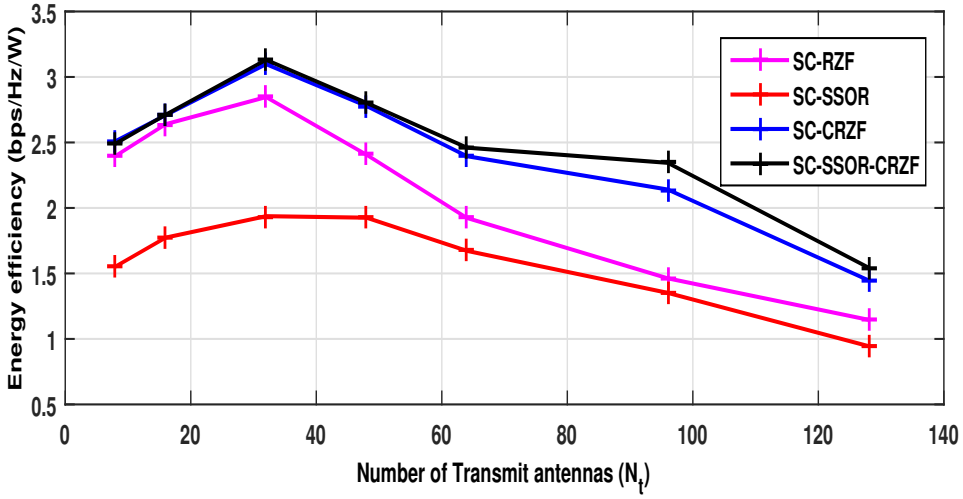

Figure 7. Energy Efficiency Variation with the No of transmitter antennas.

4.3. Impact of CSI

As far as the CSI is concerned, having the perfect knowledge of the channel state information is an ideal state of assumption, so it is always advisable to analyze the system performance under imperfect CSI conditions. The estimated channel ($\hat{H}$) with the estimation error is modelled [37] as $\hat{\mathbf{H}} = t\mathbf{H} + \sqrt{1-t^2}\mathbf{E}$. Here, $0 \leq t \leq 1$ presents the CSI accuracy and the error matrix $\mathbf{E}$ populated with the i.i.d distributed entries.

Figure 8 shows the performance of the proposed algorithm SSOR-CRZF under imperfect channel conditions. As per the simulation results, the spectral efficiency of the mmWave-mMIMO-NOMA system with SC-SSOR-CRZF HP is relatively stable from the perfect channel state information. Furthermore, with t = 0.9 and t = 0.8, the performance of the algorithm does not decrease greatly.

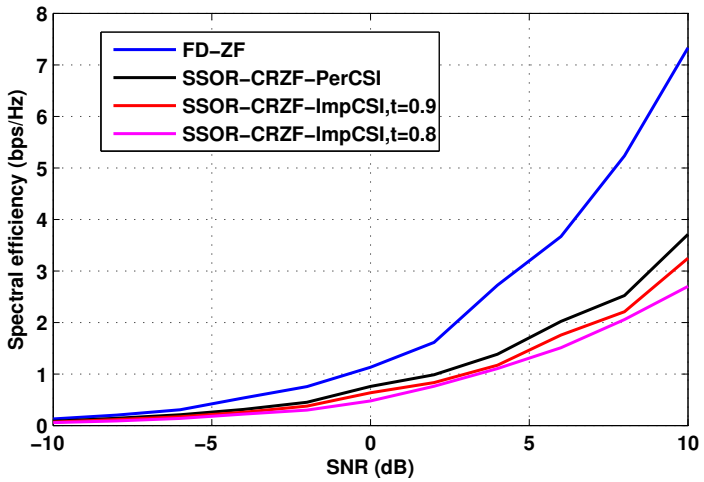

Figure 8. Impact of imperfect CSI on the proposed hybrid precoding algorithm.

5. Conclusions

This paper studied the performance of the mmWave-mMIMO-NOMA system with sub-connected architecture and under multiple user scenarios. Here, the authors have utilized the modified K-Means user grouping algorithm and then implemented the hybrid precoder. In this paper, the authors have proposed and demonstrated the performance of the

SSOR-CRZF-based hybrid precoder in terms of SE, EE, and computational complexity. The proposed SSOR-CRZF provides significant performance gain against conventional precoders like ZF, MRT, RZF, TPE, and SSOR. The SSOR-CRZF marginally improves the system performance but with reduced computation complexity in comparison to CRZF. As a part of future works, the authors would like to extend this work for energy harvesting applications.

Author Contributions: Conceptualization, S.N.S., D.K. and D.-T.D.; methodology, S.N.S., A.S. and D.T-.D.; formal analysis, A.S., N.D.N. and S.N.; writing—original draft preparation, S.N.S., D.K. and N.D.N.; writing—review and editing, S.N., A.S. and D.-T.D.; supervision, S.N. and D.-T.D.; funding acquisition, A.S. and N.D.N. All authors have read and agreed to the published version of the manuscript.

Funding: This work was supported by the FCT/MCTES through National Funds and when applicable co-funded European Union (EU) funds under Project UIDB/50008/2020-UIDP/50008/2020. The work of N.D.N. was financially supported by Van Lang University, Ho Chi Minh City, Vietnam under Project 1000.

Conflicts of Interest: The authors declare no conflict of interest.

References

1. Mumtaz, S.; Rodriguez, J.; Dai, L. *mmWave Massive MIMOA Paradigm for 5G*; Elsevier Science & Technology: Amsterdam, The Netherlands, 2016.
2. Uwaechia, A.N.; Mahyuddin, N.M.; Ain, M.F.; Latiff, N.M.A.; Za'bah, N.F. On the Spectral-Efficiency of Low-Complexity and Resolution Hybrid Precoding and Combining Transceivers for mmWave MIMO Systems. *IEEE Access* **2019**, *7*, 109259–109277. [CrossRef]
3. Heath, R.W.; Gonzalez-Prelcic, N.; Rangan, S.; Roh, W.; Sayeed, A.M. An Overview of Signal Processing Techniques for Millimeter Wave MIMO Systems. *IEEE J. Sel. Top. Signal Process.* **2016**, *10*, 436–453. [CrossRef]
4. Talaei, F.; Dong, X. Hybrid mmWave MIMO-OFDM Channel Estimation Based on the Multi-Band Sparse Structure of Channel. *IEEE Trans. Commun.* **2019**, *67*, 1018–1030. [CrossRef]
5. Ding, T.; Zhao, Y.; Li, L.; Hu, D.; Zhang, L. Hybrid Precoding for Beamspace MIMO Systems with Sub-Connected Switches: A Machine Learning Approach. *IEEE Access* **2019**, *7*, 143273–143281. [CrossRef]
6. Molisch, A.F.; Ratnam, V.V.; Han, S.; Li, Z.; Nguyen, S.L.H.; Li, L.; Haneda, K. Hybrid Beamforming for Massive MIMO: A Survey. *IEEE Commun. Mag.* **2017**, *55*, 134–141. [CrossRef]
7. Guo, Y.; Zhang, Y.; Chen, S.; Zheng, J.; Zhang, J. Hybrid Precoding for Millimeter Wave Multiuser Massive MIMO Systems with Low-Resolution DACs. In Proceedings of the 2020 IEEE 91st Vehicular Technology Conference (VTC2020-Spring), Virtual, 25–28 May 2020. [CrossRef]
8. Du, J.; Wang, Z.; Zhang, Y.; Guan, Y.; Jin, L. Multi-user hybrid precoding for mmWave massive MIMO systems with sub-connected structure. *EURASIP J. Wirel. Commun. Netw.* **2021**, *2021*, 157. [CrossRef]
9. Ayach, O.E.; Rajagopal, S.; Abu-Surra, S.; Pi, Z.; Heath, R.W. Spatially Sparse Precoding in Millimeter Wave MIMO Systems. *IEEE Trans. Wirel. Commun.* **2014**, *13*, 1499–1513. [CrossRef]
10. Mehana, A.H.; Nosratinia, A. Diversity of MIMO Linear Precoding. *IEEE Trans. Inf. Theory* **2014**, *60*, 1019–1038. [CrossRef]
11. Saleeb, B.; Shehata, M.; Mostafa, H.; Fahmy, Y. Performance Evaluation of RZF Precoding in Multi-User MIMO Systems. In Proceedings of the 2019 IEEE 62nd International Midwest Symposium on Circuits and Systems (MWSCAS), Dallas, TX, USA, 4–7 August 2019. [CrossRef]
12. Mostafa, M.; Newagy, F.; Hafez, I. Complex Regularized Zero Forcing Precoding for Massive MIMO Systems. *Wirel. Pers. Commun.* **2021**, *120*, 633–647. [CrossRef]
13. Elmagzoub, H.M. On the MMSE-based multiuser millimeter wave MIMO hybrid precoding design. *Int. J. Commun. Syst.* **2020**, *33*, e4409. [CrossRef]
14. Vizziello, A.; Savazzi, P.; Chowdhury, K.R. A Kalman Based Hybrid Precoding for Multi-User Millimeter Wave MIMO Systems. *IEEE Access* **2018**, *6*, 55712–55722. [CrossRef]
15. Ni, W.; Dong, X. Hybrid Block Diagonalization for Massive Multiuser MIMO Systems. *IEEE Trans. Commun.* **2016**, *64*, 201–211. [CrossRef]
16. Payami, S.; Ghoraishi, M.; Dianati, M. Hybrid Beamforming for Downlink Massive MIMO Systems with Multiantenna User Equipment. In Proceedings of the 2017 IEEE 86th Vehicular Technology Conference (VTC-Fall), Toronto, ON, Canada, 24–27 September 2017. [CrossRef]
17. Liu, X.; Li, X.; Cao, S.; Deng, Q.; Ran, R.; Nguyen, K.; Tingrui, P. Hybrid Precoding for Massive mmWave MIMO Systems. *IEEE Access* **2019**, *7*, 33577–33586. [CrossRef]
18. Zu, K.; de Lamare, R.C.; Haardt, M. Generalized Design of Low-Complexity Block Diagonalization Type Precoding Algorithms for Multiuser MIMO Systems. *IEEE Trans. Commun.* **2013**, *61*, 4232–4242. [CrossRef]

19. Halak, B.; El-Hajjar, M.; Hassanein, A. Hardware Efficient Architecture for Element-Based Lattice Reduction Aided K-Best Detector for MIMO Systems. *J. Sens. Actuator Netw.* **2018**, *7*, 22. [CrossRef]
20. Sur, S.N.; Bera, R.; Bhoi, A.K.; Shaik, M.; Marques, G. Capacity Analysis of Lattice Reduction Aided Equalizers for Massive MIMO Systems. *Information* **2020**, *11*, 301. [CrossRef]
21. Kandar, D.; Sur, S.N.; Singh, A.K.; Nandi, S. Performance analysis of lattice reduction-assisted precoder for multi-user millimeter wave MIMO system. *Int. J. Commun. Syst.* **2021**, *34*, e4853. [CrossRef]
22. Lyu, S.; Ling, C. Hybrid Vector Perturbation Precoding: The Blessing of Approximate Message Passing. *IEEE Trans. Signal Process.* **2019**, *67*, 178–193. [CrossRef]
23. Huang, H.; Song, Y.; Yang, J.; Gui, G.; Adachi, F. Deep-Learning-Based Millimeter-Wave Massive MIMO for Hybrid Precoding. *IEEE Trans. Veh. Technol.* **2019**, *68*, 3027–3032. [CrossRef]
24. Elbir, A.M. CNN-Based Precoder and Combiner Design in mmWave MIMO Systems. *IEEE Commun. Lett.* **2019**, *23*, 1240–1243. [CrossRef]
25. Mueller, A.; Kammoun, A.; Björnson, E.; Debbah, M. Linear precoding based on polynomial expansion: Reducing complexity in massive MIMO. *EURASIP J. Wirel. Commun. Netw.* **2016**, *2016*, 63. [CrossRef]
26. Prabhu, H.; Rodrigues, J.; Edfors, O.; Rusek, F. Approximative matrix inverse computations for very-large MIMO and applications to linear pre-coding systems. In Proceedings of the 2013 IEEE Wireless Communications and Networking Conference (WCNC), Shanghai, China, 7–10 April 2013. [CrossRef]
27. Minango, J.; de Almeida, C. A Low-Complexity Linear Precoding Algorithm Based on Jacobi Method for Massive MIMO Systems. In Proceedings of the 2018 IEEE 87th Vehicular Technology Conference (VTC Spring), Porto, Portugal, 3–6 June 2018. [CrossRef]
28. Dai, L.; Gao, X.; Su, X.; Han, S.; I, C.L.; Wang, Z. Low-Complexity Soft-Output Signal Detection Based on Gauss–Seidel Method for Uplink Multiuser Large-Scale MIMO Systems. *IEEE Trans. Veh. Technol.* **2015**, *64*, 4839–4845. [CrossRef]
29. Xie, T.; Han, Q.; Xu, H.; Qi, Z.; Shen, W. A Low-Complexity Linear Precoding Scheme Based on SOR Method for Massive MIMO Systems. In Proceedings of the 2015 IEEE 81st Vehicular Technology Conference (VTC Spring), Glasgow, UK, 11–14 May 2015. [CrossRef]
30. Xie, T.; Dai, L.; Gao, X.; Dai, X.; Zhao, Y. Low-Complexity SSOR-Based Precoding for Massive MIMO Systems. *IEEE Commun. Lett.* **2016**, *20*, 744–747. [CrossRef]
31. Zhang, L.; Hu, Y. Low Complexity WSSOR-based Linear Precoding for Massive MIMO Systems. In Proceedings of the 2016 7th International Conference on Cloud Computing and Big Data (CCBD), Macau, China, 16–18 November 2016. [CrossRef]
32. Liu, Y.; Li, Y.; Cheng, X.; Lian, Y.; Jia, Y.; Zhang, H. Low-complexity and fast-convergence linear precoding based on modified SOR for massive MIMO systems. *Digit. Signal Process.* **2020**, *107*, 102864. [CrossRef]
33. Dai, L.; Wang, B.; Peng, M.; Chen, S. Hybrid Precoding-Based Millimeter-Wave Massive MIMO-NOMA With Simultaneous Wireless Information and Power Transfer. *IEEE J. Sel. Areas Commun.* **2019**, *37*, 131–141. [CrossRef]
34. Uwaechia, A.N.; Mahyuddin, N.M. Spectrum and Energy Efficiency Optimization for Hybrid Precoding-Based SWIPT-Enabled mmWave mMIMO-NOMA Systems. *IEEE Access* **2020**, *8*, 139994–140007. [CrossRef]
35. Almers, P.; Bonek, E.; Burr, A.; Czink, N.; Debbah, M.; Degli-Esposti, V.; Hofstetter, H.; Kyösti, P.; Laurenson, D.; Matz, G.; et al. Survey of Channel and Radio Propagation Models for Wireless MIMO Systems. *EURASIP J. Wirel. Commun. Netw.* **2007**, *2007*, 1–19. [CrossRef]
36. Alkhateeb, A.; Leus, G.; Heath, R.W. Limited Feedback Hybrid Precoding for Multi-User Millimeter Wave Systems. *IEEE Trans. Wirel. Commun.* **2015**, *14*, 6481–6494. [CrossRef]
37. Rusek, F.; Persson, D.; Lau, B.K.; Larsson, E.G.; Marzetta, T.L.; Tufvesson, F. Scaling Up MIMO: Opportunities and Challenges with Very Large Arrays. *IEEE Signal Process. Mag.* **2013**, *30*, 40–60. [CrossRef]